



Spectroscopy and planetary atmospheres/Spectroscopie et atmosphères planétaires

# LIF spectroscopy applied to the study of non-thermal plasmas for atmospheric pollutant abatement

Lionel Magne\*, Stéphane Pasquiers

*Laboratoire de physique des gaz et des plasmas, université Paris-Sud, bâtiment 210, 91405 Orsay cedex, France*

Available online 3 October 2005

## Abstract

Non-thermal plasmas at atmospheric pressure are currently investigated for applications in flue gas cleaning for pollution control. Laser Induced Fluorescence (LIF) brings an irreplaceable contribution to the study of atmospheric pollutant removal kinetics, and to the monitoring of key species involved in this non-equilibrium gas phase chemistry. This article gives an overview of LIF studies in discharges for pollution control, in particular recent results obtained on NO and OH radical using a time resolved LIF diagnostic coupled to a photo-triggered discharge. Such a discharge generates transient homogeneous plasma and allows useful comparison between experimental results and predictions from a self-consistent discharge and kinetic model.

**To cite this article:** *L. Magne, S. Pasquiers, C. R. Physique 6 (2005).*

© 2005 Académie des sciences. Published by Elsevier SAS. All rights reserved.

## Résumé

**La fluorescence induite par laser appliquée à l'étude des plasmas non-thermiques pour la destruction des polluants atmosphériques.** Les plasmas non thermiques à la pression atmosphérique sont actuellement étudiés pour des applications de traitements d'effluents gazeux dans le cadre du contrôle de la pollution. La fluorescence induite par laser (FIL) apporte une contribution irremplaçable à l'étude de la cinétique de destruction des polluants et au diagnostic des espèces clés impliquées dans cette chimie hors équilibre en phase gazeuse. Cet article donne une vue d'ensemble des études menées par FIL sur des décharges appliquées à la dépollution. Des résultats récents sur NO et le radical OH obtenus par FIL résolue en temps sur une décharge photo déclenchée seront donnés. Cette décharge particulière produit un plasma pulsé homogène permettant la comparaison entre les évolutions temporelles expérimentales et les résultats d'un modèle auto cohérent de la décharge. **Pour citer cet article :** *L. Magne, S. Pasquiers, C. R. Physique 6 (2005).*

© 2005 Académie des sciences. Published by Elsevier SAS. All rights reserved.

**Keywords:** Laser Induced Fluorescence; Non-thermal plasma; Photo-triggered discharge; Volatile organic compounds; Nitrogen monoxide; Hydroxyl radical; Kinetic model

**Mots-clés :** Fluorescence Induite par Laser ; Plasma non thermique ; Décharge photo déclenchée ; Composés Organiques Volatiles ; Monoxyde d'azote ; Radical hydroxyle ; Modèle cinétique

\* Corresponding author.

*E-mail address:* [lionel.magne@pgp.u-psud.fr](mailto:lionel.magne@pgp.u-psud.fr) (L. Magne).

## 1. Introduction

Human activities are sources of many atmospheric pollutants. Abatement processes must be steadily studied and developed in order to improve elimination of gaseous wastes from the emitted effluents. In the European Community, such efforts are motivated by the more and more restrictive regulations concerning air quality. In particular, emissions of nitrogen oxides (NO and NO<sub>2</sub>) and some Volatile Organic Compounds (VOCs) will be prohibited without treatment. Various technologies already exist in gaseous effluents cleaning for pollution control. The most efficient method for VOCs elimination is total oxidation, by pyrolysis at a temperature greater than 700 °C, or by catalytic oxidation, which needs a temperature of only a few hundred Celsius degrees [1]. However, important energy consumption is needed in the case of important flows and/or low VOC concentration. Among alternative techniques presently under investigation, non-thermal equilibrium plasmas at atmospheric pressure have been studied since the end of the last century.

The effect of the non-thermal plasma in the N<sub>2</sub>/O<sub>2</sub>/pollutant(NO, VOC) mixture, with or without the addition of water molecules, is to oxidize NO or the VOC owing to reactions of O-atoms and OH-radicals with these compounds. Atoms and radicals are produced through dissociative electronic excitations of O<sub>2</sub> and H<sub>2</sub>O. Without H<sub>2</sub>O in the mixture, a high OH density can also be reached following reactions of the VOC oxidation products (the VOC is only partially oxidized). Additionally, ozone can play an important role in the oxidation process, in particular for NO at low temperature. Ozone is mainly produced through three body reactions of O with O<sub>2</sub> (+ N<sub>2</sub>). Electron beams have been first used in order to create the plasma in air at atmospheric pressure, and it has been shown that such a plasma is very efficient for the removal of most pollutants like NO<sub>x</sub> and VOCs [2]. However, pulsed electrical discharges are much better suited than electron beams for some industrial or domestic applications because they are easier to handle. Thus a growing interest has developed for the removal of pollutants using discharges [2–6]. Roughly speaking, the efficiency of a discharge to remove a pollutant from a gas stream depends mainly on:

- (i) its ability to produce large amounts of O atoms and OH radicals in the whole inter-electrode space;
- (ii) the rates of reactions of the pollutant molecule with O and OH.

It has been well demonstrated that dielectric barrier (DBD) and corona discharges fulfill the first condition [2–6]. In the case of a low oxidation reaction rate of the pollutant, the increase of the electrical energy deposited in the discharge can help in pollutant removal, but, of course, at the expense of the energy yield of the process.

Many works have shown that, even if an electrical discharge is able to convert one pollutant, this conversion is sometimes accompanied by the production of more or less harmful molecules. Usually the CO<sub>2</sub> selectivity (the ratio between CO<sub>2</sub> and CO concentrations at the exit of the reactor) is poor, namely around unity. Coupling the discharge with a catalyst had allowed one to solve some of these problems [7]. However, effluents cleaning by non-thermal plasmas has become a process with numerous parameters such as the type of pollutants, the temperature of the gas mixture, the concentrations of molecules (O<sub>2</sub>, H<sub>2</sub>O, pollutants), the electrical energy deposited in the discharge volume, the type of catalyst, etc. Moreover, as far as DBD or corona discharges are concerned, the electrical energy deposition in air at atmospheric pressure is strongly non-homogeneous. These discharges are characterized by micro-filaments of plasmas. Therefore another important parameter, whose role has been more recently focused upon [8,9], is the spatial and temporal repartition of the energy deposition in the discharge.

Optimization of the process cannot be achieved without numerous experiments and without physical and chemical modeling which should help design efficient cleaning reactors. Previously to their exploitation, kinetic models must be developed and validated through comparisons of their predictions with measurements on the various chemical species, radicals and molecules, which are created in the discharge and in the flowing afterglow (spatio-temporal post-discharge), using specifically designed experiments. Usually FTIR spectroscopy and chromatography techniques are used to characterize the gas mixture composition at the exit of the discharge. These *ex situ* experimental diagnostics allow the identification of molecules and the determination of their concentrations, but transient radicals involved in the kinetic path of the pollutant removal can not be monitored in this way. On the other hand, the chemistry in the vicinity of a single micro-filament of plasma deserves to be studied as accurately as possible, both with respect to radicals and molecules, in order to achieve a comprehensive understanding of the reactive medium. The only way to perform such spatially and temporally resolved *in situ* studies is to use laser spectroscopy techniques, in particular the Laser Induced Fluorescence (LIF) which allows local non-disturbing measurements of chemical species densities. This is a quite hard task, because a strongly non-homogeneous transient high pressure plasma is concerned. However, some works have been performed these last years on N and O atoms, OH radicals, and NO molecules [10–19].

Even if some LIF measurements have been performed in filamentary discharges such as DBD or corona, a reliable kinetic interpretation of experimental data on atoms and radicals is not easy to obtain. Indeed, it requires a self-consistent modeling of both the streamer propagation physics and the chemistry involved in the gas mixture under consideration, for which a lot of reactions must be taken into account. This is a very important point, in particular, as far as VOCs are concerned, because of many by-products following the oxidation of the pollutant molecule. In order to make easier measurements, and to achieve more reliable comparisons between kinetic modeling predictions and experimental results, we have implemented the LIF diagnostic

on a photo-triggered discharge reactor in order to determine the time evolution of radicals and pollutant molecules densities in the reactive afterglow. The photo-triggering technique allows us to achieve homogeneous transient high-pressure plasmas in various types of gas mixtures [20]. Therefore, measurements are compared to predictions of a self-consistent 0D discharge and kinetic model, which takes into account all relevant reactions for radicals and molecules.

After a short description of DBD and corona discharges, the first part of this article briefly resumes the few published LIF experiments performed in filamentary discharges. Thereafter, the second part is devoted to measurements in the photo-triggered discharge, on the NO molecule and on the OH radical. The contribution of the LIF diagnostic to the understanding of the plasma kinetic is emphasized through some selected comparisons of model predictions with experimental results.

## 2. Laser Induced Fluorescence applied to filamentary discharges

### 2.1. Short physical description of DBD and corona discharges

Atmospheric pressure non-thermal plasmas generated by DBD or corona discharges have been the subject of a very abundant literature since the first work by Siemens in the mid nineteenth century [21]. Such plasmas can be created by the application of a pulsed or a sinusoidal high voltage between two electrodes, whose gap is filled with the gas. As a quick description, DBD and corona discharges consists of conductive micro-filaments which are established following the propagation of ionization fronts, usually called streamers, in multiple places in the discharge volume. These filaments have a very short lifetime, of the order of a few tens of nanoseconds. Each one is a narrow cylindrical plasma channel (radius of the order of 100  $\mu\text{m}$ ). The exchange of energy between electrons and molecules takes place mainly during the phase of discharge development, namely during the propagation of the streamers. Energetic electrons are created in streamers, which excite the molecules and then transform a share of their kinetic energy into energy stored by excited species and free radicals (by dissociation of molecules).

It is known that the critical reduced electric field,  $(E/N)_C$  ( $N$ , the total gas density), corresponding to equal electron production through ionisation processes and losses through attachment on oxygen or water molecules in air is about 100 Td [22] (1 Td =  $10^{17}$  V·cm<sup>2</sup>). As a result, the minimum voltage value to apply between two plane electrodes is about 25 kV/cm in order to achieve discharge breakdown; lower voltage values can be used in case of non-planar electrodes (tips, wires, ...) owing to the field enhancement near the metallic surface. This explains that the inter-electrode distance for most of the plasma reactors designed for gas cleaning which have been studied up to now, is around 1 cm or less. Without a dielectric material placed on one of the electrodes, i.e., for corona discharge, the duration of application of the voltage has to be very short, typically 10 ns which is the time for the propagation of streamers in the inter-electrode gap [22]. For a longer time value the electrical energy is only deposited in the very small diameter high current channel corresponding to the thermal plasma of an arc, which is not desirable for an efficient pollutant removal. On the contrary, the voltage pulse duration used to generate the dielectric barrier discharge can be much longer, for example 1  $\mu\text{s}$ , without the appearance of arcs. In this case electric charges are locally deposited on the dielectric surface when one streamer reaches it, so that the non-thermal plasma filament which follows the streamer propagation disappears very rapidly owing to the low electric field value, much less than  $(E/N)_C$ , in this conducting channel. The current pulse duration is only some tens of nanoseconds at maximum because the discharge completely extinguished when electric charges are uniformly distributed on the surface, the discharge being characterized by a lot of plasma filaments randomly distributed in the whole inter-electrode space [23]. The electrical energy deposited in the discharge, per voltage pulse, is usually relatively low, for example in the range 10–100 mJ. However, the discharge can work at a high repetition frequency (at the present time high voltage supply units are developed with a repetition frequency up to 100 kHz).

### 2.2. LIF detection of atoms, radicals, and molecules in and around micro-filaments of plasma

To the authors' knowledge, there is only one work about LIF on atoms in filamentary discharge. Two-photon Absorption LIF (TALIF) has been applied by Lukas et al. [11] to detect N and O atoms in a DBD. These authors have performed very nice space and time resolved measurements of the relative atomic density distributions at a single plasma filament with submillimetre radial dimensions. These authors use a laser wavelength of 207 nm for N, and of 226 nm for O.

Concerning radicals, a few works have been performed on OH in high pressure non-thermal plasmas. The first to be published was by Ershov and Borysow [24], but the discharge studied is not filamentary. It is a DC low current (10 A) pulsed discharge (duration between 0.2 and 50  $\mu\text{s}$ ) working with an electrode spacing of three millimeters, without dielectric material. The plasma created by such a discharge is homogeneous owing to the use of a pre-ionization achieved by a continuous discharge of very weak current level (10 mA). Transitions employed for the one photon LIF excitation are in the same band than that we use for investigations on the OH kinetic in the photo-triggered discharge, see Section 3.3. Following the pioneer work by Ershov and Borysow, several research groups have applied the LIF technique to detect OH in filamentary discharges, either DBD or corona [12–14]. Amongst those, Ono and Oda [14] have applied a different excitation scheme. Following previous works in

combustion research, these authors used a KrF laser (248 nm) to excite the radical in a state where pre-dissociation dominates over all relaxation processes. It has the advantage that the undesirable influence of the quenching in the excited state is reduced, so that the absolute density of OH in its ground state can be estimated in the non-homogeneous plasma.

Ono and Oda [18] have also studied NO formation in a pulsed spark discharge in  $N_2/O_2/Ar$  mixture at atmospheric pressure. Again the emission of a KrF laser is used to excite the nitrogen oxide molecule. Other works deal with removal processes of NO observed by LIF imaging spectroscopy, which allows one to measure the two-dimensional distribution of the pollutant density around the plasma filament generated in needle-to-plane discharges [15–17,19]. For these experiments an excitation transition at 226 nm is used, as in our works on photo-triggered discharges, see Section 3.2.

### 3. Laser Induced Fluorescence applied to the photo-triggered discharge

Formerly designed for the development of high-power lasers [25,26], the photo-triggering technique has been more recently applied to gas mixtures ( $N_2/O_2/H_2O$ ) relevant for atmospheric pollutant removal, such as NO [27] or light olefins [28]. We have undertaken, for a few years, basic research on the high-pressure non-thermal plasma chemistry using time resolved LIF diagnostic coupled to photo-triggered discharge. The NO removal in reductive mixtures  $N_2/H_2O/C_2H_4/NO$  [29,30], the production mechanisms and reactivity of OH radical in the  $N_2/H_2O$  mixture [31], as well as in  $N_2/O_2$  containing a light unsaturated ( $C_2H_4$ ) or a saturated ( $C_2H_6$ ) hydrocarbon [32,33], or acetaldehyde ( $CH_3CHO$ ) [34], have been studied.

#### 3.1. The photo-triggered discharge reactor for LIF experiments

A comprehensive description of the photo-triggered discharge operating mode has been previously described in detail [20, 25–27] and only a brief description of our device is given here. Two electrodes, 50 cm long with a spacing  $d = 1$  cm and a flat profile over 1 cm width, are directly connected to an energy storage unit of capacitance  $C = 17.44$  nF charged up to a voltage  $V_0$  in a few hundred nanoseconds. Once  $V_0$  is reached on the electrodes, gas breakdown is achieved through photo-ionisation of the gas mixture by UV-photons which are produced by an auxiliary corona discharge located at the bottom of the main discharge.

A gas compressor is used to produce a gas flow through the discharge gap. The discharge frequency, 1.25 Hz, is chosen such that the whole reactor volume,  $500\text{ cm}^3$ , is renewed between two discharges. The total pressure of the studied mixtures has been varied from 230 up to 460 mbar, and the initially applied reduced electric field between the gap,  $(E/N)_0$ , given by  $(E/N)_0 = V_0/(dN)$  where  $N$  is the total density of the gas mixture, ranging from 150 up to 350 Td in our experiment. Control of water in the discharge vessel is obtained with a mixture of dry nitrogen and nitrogen saturated with water vapour (concentration of 3.3% at 298 K and atmospheric pressure). NO and  $H_2O$  maximum concentration values are respectively equal to 1000 ppm and 2.5%, at ambient temperature. Oxygen and VOC (ethene, ethane, acetaldehyde) molecule concentrations are 5% and in the range 250–5000 ppm, respectively.

The low discharge circuit inductance, 6.5 nH, allows us to obtain a short current pulse duration of 60 ns. The deposited energy in the discharge ranges from 1.1 up to 4.6 J. Details of the time resolved measurement technique in the afterglow have been previously published [35]. We use a Datachrom 5000 system from Quantel including a tunable dye laser TDL50 pumped by a pulsed Nd:Yag laser. The pulse width is 7 ns. Fluorescence is observed at a point in the 50 cm long homogeneous afterglow volume, from 1 up to 200  $\mu\text{s}$  after the current pulse, using an adapted synchronization device between the pre-ionisation pulse and the laser shot. The fluorescence light emitted from a small volume of plasma (diameter  $\sim 4$  mm, length  $\sim 4$  mm) is focused on the entrance slit of a monochromator (Jobin Yvon HR 640) by a 15 cm focal length lens. This monochromator is used as a broadband filter. The entrance and exit slits are opened to obtain a bandwidth of 1.5 nm in order to spectrally integrate the LIF emission. The electrical signal from a photo-multiplier tube (Hamamatsu R928) is time-integrated, during the scan of the laser wavelength, by a boxcar system (EG&G 4402) working in live mode without pre-averaging (gate width of some tens of nanoseconds).

#### 3.2. The LIF diagnostic for detection of the NO molecule

For the detection of NO, the Nd:Yag emission at 1064 nm is frequency doubled in a KDP crystal. This green emission (532 nm) pumps a rhodamine 590/610 mixture to generate emission around 574 nm. In the next step, the dye laser frequency is first doubled in a second KDP crystal and then mixed to the 1064 nm wavelength to give an emission around 226 nm, corresponding to the  $X^2\Pi \rightarrow A^2\Sigma$  excitation transition of NO. At 226 nm the laser line width given by the laser manufacturer is about  $6 \times 10^{-4}$  nm. In fact, the actual line-width is certainly higher, as is attested by the multi-mode working that is detected by the double resonance observed in LIF signals of single molecular lines. The laser energy by pulse is of about 0.6 mJ for a beam diameter of 4 mm at the laser output. Beam energy at the cell entrance is of about 0.2 mJ after attenuation by fused silica plates.

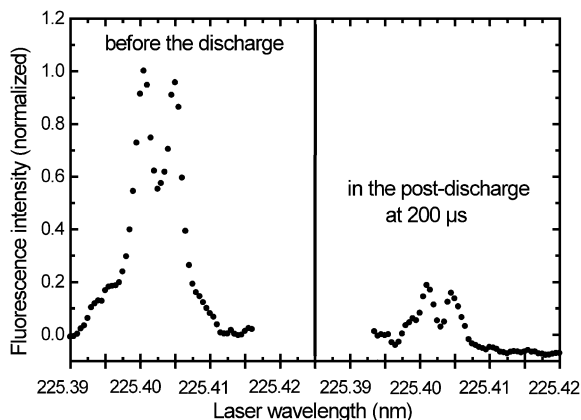


Fig. 1. LIF measurements of NO in N<sub>2</sub>/NO mixtures before discharge and 200 μs after discharge.

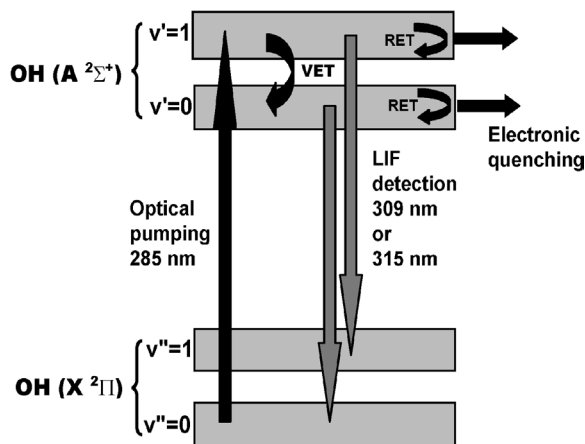


Fig. 2. Excitation and detection scheme for LIF diagnostic of OH. RET, VET and quenching are taken into account in the LASKIN simulation program.

Typical examples of LIF measurements are given on Fig. 1. On the left side of the diagram is plotted the normalized fluorescence intensity measured from the non-excited mixture of gases, namely N<sub>2</sub>/NO, and on the right side the intensity measured from the post-discharge. Typical fluctuation of the signal peak value is in the range ±10%.

### 3.3. The LIF diagnostic for detection of the OH radical

The excitation and detection scheme adopted for the OH radical is presented in Fig. 2. This figure also presents the collisional processes of the concerned levels. The fastest processes are the rotational energy transfers (RET). For the levels OH(X<sup>2</sup>Π, v' = 0), OH(A<sup>2</sup>Σ<sup>+</sup>, v'' = 0) and OH(A<sup>2</sup>Σ<sup>+</sup>, v'' = 1), these processes can be written as follows:



where  $E$  corresponds to the electronic level,  $v$  and  $N$  are respectively the vibrational and rotational quantum numbers. During the RET process, only the rotational quantum number is changed during the collision with the collider  $M$ ; N<sub>2</sub> and O<sub>2</sub> molecules, and eventually H<sub>2</sub>O in case of a wet gas mixture, are the main colliders in the conditions of our experiments. Vibrational energy transfers (VET) from OH(A<sup>2</sup>Σ<sup>+</sup>, v = 1) to OH(A<sup>2</sup>Σ<sup>+</sup>, v = 0) are:



Other lost terms of the A<sup>2</sup>Σ<sup>+</sup> state feeding OH(X<sup>2</sup>Π, v = 0) are electronic quenching (EQ) of OH(A<sup>2</sup>Σ<sup>+</sup>, v = 1) and OH(A<sup>2</sup>Σ<sup>+</sup>, v = 0).

As shown in Fig. 2 we excite the radical in the ultraviolet range on the A → X system, using the (1, 0) band excitation around 285 nm. For this purpose the rhodamine 590/610 mixture provides an emission around 570 nm which is frequency doubled with a KDP crystal to obtain the required wavelength at 285 nm. For this arrangement the line width is about 0.1 cm<sup>-1</sup> (constructor data). The maximum surface section of the beam is about 5 mm<sup>2</sup> and the energy by pulse can be varied from 0.5 up to 10 mJ using optical attenuators.

The optical pumping is set on the P<sub>2</sub>(6) transition which feeds the F<sub>2</sub>(5) rotational level of OH(A<sup>2</sup>Σ<sup>+</sup>, v'' = 1) from the F<sub>2</sub>(6) rotational level of OH(X<sup>2</sup>Π, v = 0), and we detect the fluorescence on the (0, 0) band. This band gives a stronger emission than the (1, 1) band at 315 nm. To get a comprehensive explanation for this effect, we have used the LASKIN simulation program [36] for time resolved LIF spectra under full consideration of the collisionally induced energy transfer processes (RET, VET and quenching) and predissociation as well as spontaneous emission. Fig. 3 shows rotational distributions for OH(A<sup>2</sup>Σ<sup>+</sup>, v'' = 1) and OH(A<sup>2</sup>Σ<sup>+</sup>, v'' = 0) integrated during the optical pumping. Collisional processes have been taken into account for a N<sub>2</sub>/O<sub>2</sub> bath mixture with 5% of oxygen at a total pressure of 460 mbar and at ambient temperature. It can be seen that the integrated population of OH(A<sup>2</sup>Σ<sup>+</sup>, v' = 1) is lower than OH(A<sup>2</sup>Σ<sup>+</sup>, v' = 0) one. This is in very good agreement with measurements, i.e., the (0, 0) band at 309 nm offers the strongest emission. This strong emission at the expense of the (1, 1) band is now explained by the losses of OH(A<sup>2</sup>Σ<sup>+</sup>, v' = 1) by VET which are faster than electronic quenching of OH(A<sup>2</sup>Σ<sup>+</sup>, v'' = 0). This leads to a higher population of OH(A<sup>2</sup>Σ<sup>+</sup>, v'' = 0) which then gives the dominating emission.

Fig. 4 resumes the OH excitation and detection scheme with respect to the laser (on the left side of the diagram) and LIF emission (on the right side) wavelengths. Motivation for the choice of the P<sub>2</sub>(6) excitation transition is the low value of the

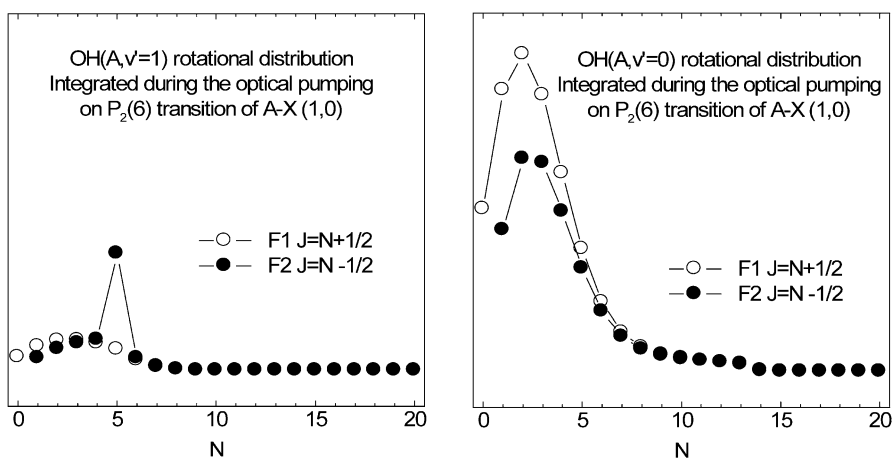


Fig. 3. LASKIN calculation of OH( $A, v' = 1$ ) and OH( $A, v' = 0$ ) rotational distributions integrated during the laser pulse. Optical pumping was tuned to the  $P_2(6)$  transition of  $A-X(1,0)$  band. Collisional processes were computed for a  $N_2/O_2$  bath mixture with 5% of  $O_2$  at a total pressure equal to 460 mbar at 300 K.

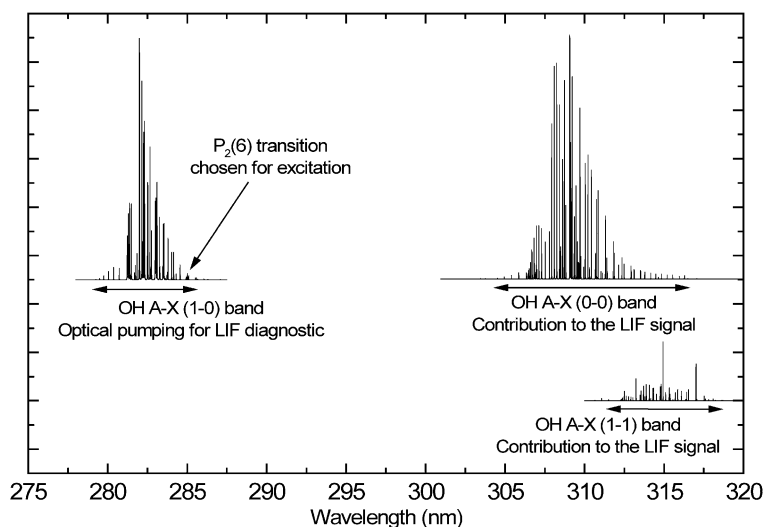


Fig. 4. Calculation of excitation and fluorescence spectra of OH. Relative contribution of (0, 0) and (1, 1) band to the LIF signal were calculated consistently with the rotational distributions plotted in Fig. 3.

corresponding oscillator strength and the low population on level  $F_2(6)$  so that the laser beam energy loss by absorption on the optical path before the detection volume is negligible. We recall that the LIF-emission is integrated by the boxcar, but we have plotted in Fig. 4 the emission lines intensities for both the (0, 0) and (1, 1) bands corresponding to the calculated rotational distributions plotted in Fig. 3; as discussed above the first is higher than the second. In order to follow the time evolution of the OH density in the discharge afterglow, measurements have been made by scanning the whole resonance of the  $P_2(6)$  transition to accurately determine the value of the LIF signal at the center of the resonance. An example measurement is displayed in Fig. 5, i.e., the boxcar integrated LIF signal versus the laser wavelength, for the  $P_2(6)$  and its neighboring the  $P_{12}(6)$  lines.

### 3.4. Coupling of the time resolved LIF to the photo-triggered discharge: a powerful tool to study high pressure non-thermal plasma kinetics

In this section we will focus on the contribution of the LIF diagnostic, applied to the photo-triggered discharge, to the understanding of the plasma kinetic [29–35]. Let us examine first the case of the NO molecule. Fig. 6 displays an example of the experimental time evolution of the NO density during the post discharge, in the  $N_2/NO$  mixture (circles) and with addition of 2.1% of  $H_2O$  (triangles). The total pressure is 460 mbar, the initial NO density is  $1.1 \times 10^{16} \text{ cm}^{-3}$  (1000 ppm), and the applied

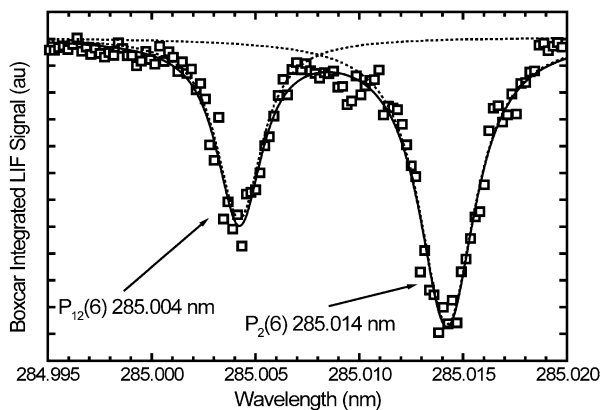


Fig. 5. Experimental LIF spectrum for  $\text{OH}(X^2\Pi, v'' = 0) \rightarrow \text{OH}(A^2\Sigma^+, v' = 1)$  excitation obtained for  $[\text{C}_2\text{H}_4] = 5000$  ppm at  $t = 10 \mu\text{s}$  in the post-discharge.

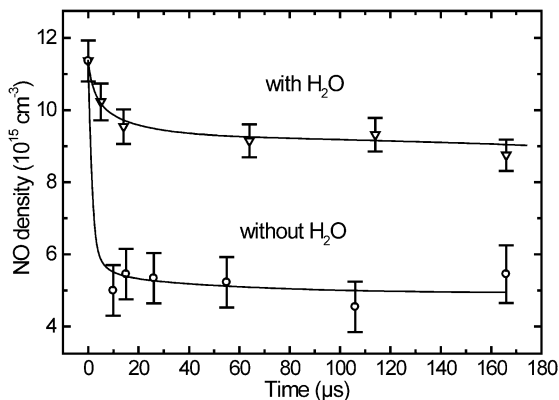


Fig. 6. Evolutions of NO density in the time afterglow in  $\text{N}_2/\text{NO}$  mixture (circles) and with addition of 2.1% of  $\text{H}_2\text{O}$  (triangles).

voltage is 23 kV which gives an initially applied reduced electric field of about 200 Td (deposited energy: 4.6 J, specific energy: 92 J/l). Measurements in this figure emphasize that NO density rapidly decreases in both mixtures so that a stationary-state is achieved about 10  $\mu\text{s}$  after the discharge. In this state, the percentages of NO destroyed are 25% and 60% with and without  $\text{H}_2\text{O}$  respectively, for the chosen conditions.

The strong effect of water addition on NO removal efficiency is due to the quenching of singlet metastable states of the nitrogen molecule,  $\text{N}_2(a^1\Sigma)$ ,  $\text{N}_2(a^1\Pi)$  and  $\text{N}_2(w^1\Delta)$ , which are strongly mixed by collisions and are further called  $\text{N}_2(a')$  in the following:



It has been demonstrated in [30] through comparisons of predictions of a self-consistent discharge and kinetic model with experimental results. In the dry mixture, it is known that the NO removal is explained by two kinetic processes [29]. Firstly,  $\text{N}_2(a')$  states are involved through the dissociative process:



Secondly, NO is reduced by N atoms which are produced both by dissociative electron collisions on  $\text{N}_2$  and by reaction (2), i.e.,



which is a well-known process, very often invoked to explain NO-removal in the so-called reductive gas phase [2,5], i.e. without molecular oxygen in the initial mixture. The LIF diagnostic applied to the photo-triggered discharge clearly emphasizes, as shown in Fig. 6, that the addition of  $\text{H}_2\text{O}$  to the  $\text{N}_2/\text{NO}$  mixture decreases drastically the NO removal. The loss of singlet metastable states, reaction (1), leads to a decrease in the frequency of reaction (2) in such a way that the NO removal can be considerably lowered. This result is very similar to that we have previously obtained on the effect of addition of a light hydrocarbon,  $\text{C}_2\text{H}_4$  [29]. Quenching reactions of  $\text{N}_2(a')$  by water or ethene molecules have been invoked for the first time following works on the photo-triggered discharge.

For molecules of the type  $\text{C}_x\text{H}_y\text{O}_z$ , the OH radical is known to be one of the most important reactive species involved in the removal of the pollutant. In case of wet air, this radical is produced during the discharge by dissociative electron collisions on  $\text{H}_2\text{O}$ . Thereafter OH reacts with the VOC according to the following two body or three body collision process:

– H-atom abstraction:



which occurs, for example, for saturated hydrocarbons, aldehydes, or alcohols:

– OH addition:



which occurs for unsaturated hydrocarbons. On the other hand, in dry air, the first step of the VOC removal is the molecule oxidation by O-atoms, i.e.,



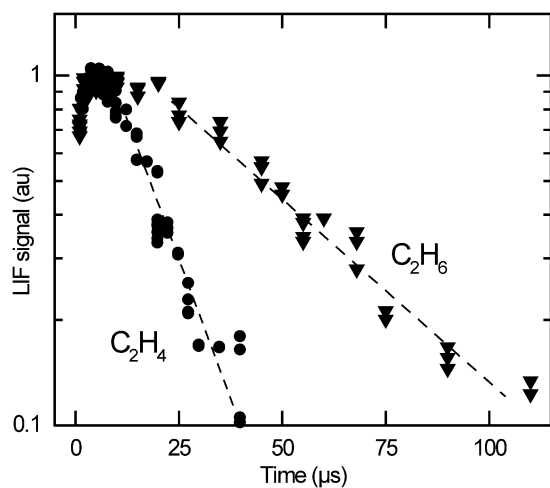


Fig. 7. Evolutions of OH density in the time afterglow for  $N_2/O_2$  mixture with 5% of  $O_2$  and addition of 5000 ppm of  $C_2H_4$  (circles) or 5000 ppm of  $C_2H_6$  (triangles). Total pressure is 460 mbar.

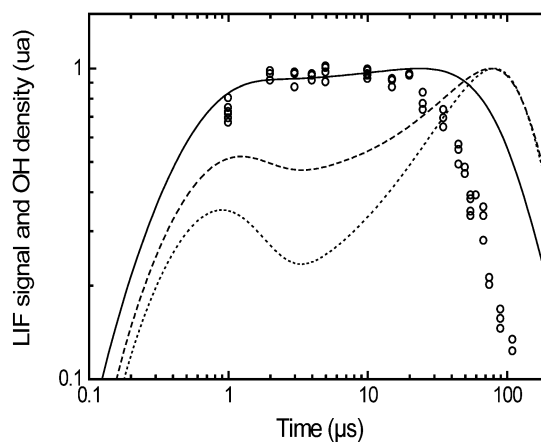


Fig. 8. Comparison between experimental OH density evolution and results of self-consistent modelling for different kinetic schemes (see text).

The hydroxyl radical can be either directly produced (H abstraction) by reaction (5) or appears in the energized gas mixture following a complex reaction scheme which involves the products of this reaction. It is followed by reaction (4a) or (4b) during the afterglow, after deposition of the electrical energy during the discharge. The relative importance of reactions (4) and (5) in the removal of the VOC should be very difficult to determine in the case of filamentary discharges, and the contribution of other reactions to the production and loss processes of OH should be hardly estimated. As discussed below, the use of the photo-triggered discharge coupled to the time resolved LIF on the OH radical has allowed us to get some new information about kinetic processes for this important transient specie [32–34].

In Fig. 7 are plotted some experimental results obtained for the time evolution of the OH density in the photo-triggered discharge afterglow. The mixture of gases consists of  $N_2$  with 5%  $O_2$  and 5000 ppm of either ethene or ethane, at a total pressure of 460 mbar. Electrical discharge parameters are identical to those of Fig. 6. It can be seen that the radical density increases rapidly after the discharge, the maximum being achieved at about 10  $\mu s$ . Despite  $H_2O$  is not initially present in the mixtures, such a rapid increase has been encountered with the two hydrocarbons studied (time of the maximum LIF signal between 10 to 20  $\mu s$ , depending on the molecule and on the initial concentration), and also with acetaldehyde. After 25  $\mu s$ , the signal exhibits a quasi exponential decrease, and the corresponding characteristic frequency increases when ethane is replaced by ethene. It is also the case when the concentration of one of these compounds is increased. Similar results have been obtained with acetaldehyde.

Interpretation of experimental data such as those plotted in Fig. 7 cannot be obtained looking only at the oxidation kinetics of the pollutant molecules. Indeed, oxidation processes of  $C_2H_4$  and  $C_2H_6$  by O atoms are very different [37] and, as a consequence, production rates of OH *should be* very different in the two mixtures  $N_2/O_2/C_2H_4$  and  $N_2/O_2/C_2H_6$ . However, it is not the case, the maximum of the OH density being located nearly at the same time in the afterglow for given electrical parameters of the discharge.

In Fig. 8 are plotted kinetic model results together with experimental results for 5000 ppm of ethane. Three different kinetic schemes are emphasised on this figure. The first (dotted line) corresponds to the hypothesis that dissociative electronic collisions on  $C_2H_6$  (both optically forbidden and allowed transitions) do not produce H-atoms, i.e.,



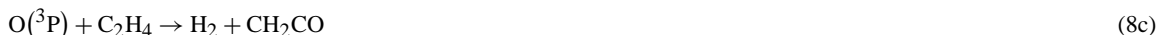
Moreover the rate constant for H and O atom recombination,



is taken from the review article by Tsang and Hampson [38],  $k = 1.3 \times 10^{-29} T^{-1} \text{ cm}^6 \text{ s}^{-1}$ , where T is the temperature in K. To the authors' knowledge, no other determination of this coefficient has been published more recently. Clearly, the time evolution of the OH density computed using such a kinetic scheme exhibits a large discrepancy as compared with measurements. In particular a minimum density is predicted at 3  $\mu s$ , which is not seen in the experiment. In the second scheme (dashed line in Fig. 8), we assume that dissociation of ethane, reaction (6), only produces H-atoms and  $C_2H_5$  radicals. As a result the minimum

OH density is less important but still exists. For both schemes the maximum density is reached at about 80  $\mu\text{s}$ , which is far from experimental results. In the third scheme (full line), the rate constant for reaction (7) has been increased by a factor 100, also taking into account H-atom production through ethane dissociation by electronic collisions. In this way predictions and experimental points agree for time values less than 20  $\mu\text{s}$ . In particular, the OH density is quasi constant between 2 and 20  $\mu\text{s}$ , the maximum value being  $3.1 \times 10^{14} \text{ cm}^{-3}$ . As previously mentioned by Tsang and Hampson [38], the numbers given in the literature for the rate of reaction (7) are rough estimates. In an older work, Baulch et al. [39] have summarised them, giving a range from  $10^{-33}$  to  $10^{-30} \text{ cm}^{-3}$ . The value taken into account in the third computation presented above corresponds to the upper limit of this range.

In the  $\text{N}_2/\text{O}_2/\text{C}_2\text{H}_4$  mixture, OH is produced after partial oxidation processes of the hydrocarbon,



and reactions of the oxidation by-products. Very shortly after the discharge, a few tens of ns after the current pulse, the HCO radical is the main precursor for OH creation through the two reactions:



and



However reaction (7) rapidly dominates with respect to (10), and becomes the most important OH production process. After about 10  $\mu\text{s}$  (times given here are only indicative, exact values depending on the ethene concentration), two other reactions dominate, firstly:



until 100  $\mu\text{s}$  and, secondly:



The  $\text{HO}_2$ ,  $\text{CH}_2\text{OH}$  and  $\text{CH}_3\text{O}_2$  radicals are produced through a number of reactions which are too numerous to be described in detail here. On the other hand, the hydrogen atom is mainly produced, at short times ( $< 1 \mu\text{s}$ ) and late times ( $> 30 \mu\text{s}$ ), by the oxidation reaction (8a), whereas the reaction of the oxygen atom with OH giving  $\text{O}_2$  and H dominates between 1 and 30  $\mu\text{s}$ .

The maximum value of the OH density obtained for the mixture with ethene (for example,  $1.56 \times 10^{15} \text{ cm}^{-3}$  at 5000 ppm initial hydrocarbon concentration) is higher than the one for the mixture with ethane ( $3.1 \times 10^{14} \text{ cm}^{-3}$ ), owing to the more important reactivity of the first (because it is with an unsaturated HC) compared to the second (saturated HC).

To summarize, agreement between experimental and calculated OH density time evolutions has been found for  $\text{N}_2/\text{O}_2$  mixtures containing ethane or ethene, assuming that: (i) dissociative electronic excitation of  $\text{C}_2\text{H}_6$  mostly produces H-atoms; (ii) the rate for recombination of O and H atoms through three body collisions is about  $3 \times 10^{-30} \text{ cm}^6 \text{ s}^{-1}$  at 300 K. These results are consistent with studies on the mixture with acetaldehyde at low concentration of the pollutant molecule [34].

#### 4. Conclusion

Up to now, use of the Laser Induced Fluorescence technique remains the better way to study the dynamic of atmospheric pollutant removal by non-thermal plasmas, because it is a non-disturbing technique which can be spatially and temporally resolved with characteristics consistent with the physics of micro-filaments of plasmas in dielectric barrier or corona discharges. However, it is not so easy to handle on such non-homogeneous transient reactive media, and analysis of experimental results are hindered because it requires a self-consistent modeling of both the streamer propagation physics and the chemistry involved in the molecular gas mixture, for which many reactions must be taken into account. The results summarized above emphasize that coupling of the time resolved LIF technique to the photo-triggered discharge is a very useful diagnostic tool to study molecule and radical kinetics in high pressure non-thermal plasmas, in particular for OH, which is a key species for the removal of VOCs of the type  $\text{C}_x\text{H}_y\text{O}_z$ . The interpretation of experimental results can be achieved with the help of a self-consistent 0D-model of the discharge including all relevant chemical processes for the studied mixtures.

## Acknowledgements

The authors are indebted to their colleague G. Baravian, research engineer now retired, for very significant participation to LIF experiments on the photo-triggered discharge. G. Baravian was amongst the first to use LIF and TALIF as a diagnostic technique in non-thermal plasmas. Members of the team *Décharges Impulsionnelles de Puissance* at LPGP, Orsay, are also greatly acknowledged, in particular V. Puech and C. Postel. This article is dedicated to the memory of G. Gousset, former director of LPGP.

## References

- [1] S. Vigneron, E. Caverne, O. Schwebel, in: P. Le Cloirec (Ed.), *Les Composés Organiques Volatils dans l'Environnement*, Lavoisier Tech. Doc., Paris, 1998, p. 305.
- [2] B. Penetrante, S. Schultheis (Eds.), *Non Thermal Plasma Techniques for Pollution Control (parts A and B)*, Springer-Verlag, Berlin, 1993.
- [3] Th. Hammer, *Contrib. Plasma Phys.* 39 (1999) 441.
- [4] L. Rosocha, R. Korzekwa, *J. Adv. Oxid. Technol.* 4 (1999) 247.
- [5] E.-M. Van Veldhuizen (Ed.), *Electrical Discharges for Environmental Purposes, Fundamentals and Applications*, NOVA Science Publishers, New York, 2000.
- [6] K. Yan, E. van Heesch, A. Peme, P. Huijbrechts, *Plasma Chem. Plasma Proc.* 21 (2001) 107.
- [7] S. Pasquiers, *Europ. Phys. J. Appl. Phys.* 28 (2004) 319.
- [8] A. Khacef, J.-M. Cormier, J.-M. Pouvesle, in: *XVI International Symposium on Plasma Chemistry, Taormina, Italy (22–27/06/2003)*.
- [9] J. Jarrige, N. Blin-Simiand, F. Jorand, L. Magne, S. Pasquiers, C. Postel, in: *XV International Symposium on Plasma Chemistry, Toronto, Canada (7–14/08/2005)*.
- [10] M. Spaan, Ch. Lukas, V. Schulz-von-der-Gathen, H. Döbele, in: *Frontiers in Low Temperature Plasma Diagnostics III*, Saillon, Swiss (15–19/02/1999).
- [11] Ch. Lukas, M. Spaan, V. Schulz-von-der-Gathen, M. Thomson, R. Wegst, H. Döbele, M. Neiger, *Plasma Sources Sci. Technol.* 10 (2001) 445.
- [12] R. Sankaranarayanan, B. Pashaie, S. Dhali, *Appl. Phys. Lett.* 77 (2000) 2970.
- [13] R. Kleinhans, L. Tiase, V. Beushausen, in: *ICOPS 2000, New Orleans, USA (4–7/06/2000)*.
- [14] R. Ono, T. Oda, *J. Phys. D* 35 (2002) 2133.
- [15] G. Roth, A. Gundersen, *IEEE Trans. Plasmas Sci.* 27 (1999) 28.
- [16] H. Hazama, M. Fujiwara, M. Tanimoto, *Chem. Phys. Lett.* 323 (2000) 542.
- [17] S. Kanazawa, T. Ito, Y. Shuto, T. Ohkubo, Y. Nomoto, J. Mizeraczyk, *IEEE Trans. Ind. Appl.* 37 (2001) 1663.
- [18] R. Ono, T. Oda, *J. Phys. D* 35 (2002) 543.
- [19] S. Kanazawa, T. Sumi, S. Shimamoto, T. Ohkubo, Y. Nomoto, M. Kocik, J. Mizeraczyk, J.-S. Chang, *IEEE Trans. Plasmas Sci.* 32 (2004) 25.
- [20] B. Lacour, V. Puech, S. Pasquiers, *Recent. Res. Devel. Appl. Phys.* 6 (2003) 149.
- [21] W. Siemens, *Poggendorffs Ann. Phys. Chem.* 102 (1857) 66.
- [22] Y. Raizer, *Gas Discharge Physics*, Springer-Verlag, Berlin, 1991.
- [23] B. Eliasson, U. Kogelschatz, *IEEE Trans. Plasma Sci.* 19 (1991) 309.
- [24] A. Ershov, J. Borysow, *J. Phys. D* 28 (1995) 68.
- [25] R. Riva, M. Legentil, S. Pasquiers, V. Puech, *J. Phys. D* 28 (1995) 856.
- [26] B. Lacour, S. Pasquiers, C. Postel, V. Puech, *Appl. Phys. B* 72 (2001) 289.
- [27] M. Rozoy, C. Postel, V. Puech, *Plasma Sources Sci. Technol.* 8 (1999) 337.
- [28] S. Pasquiers, C. Postel, L. Magne, V. Puech, G. Lombardi, *J. Adv. Oxid. Technol.* 7 (2004) 108.
- [29] F. Fresnet, G. Baravian, L. Magne, S. Pasquiers, C. Postel, V. Puech, A. Rousseau, *Appl. Phys. Lett.* 77 (2000) 4118.
- [30] F. Fresnet, G. Baravian, L. Magne, S. Pasquiers, C. Postel, V. Puech, A. Rousseau, *Plasma Sources Sci. Technol.* 11 (2002) 152.
- [31] G. Baravian, F. Fresnet, L. Magne, S. Pasquiers, C. Postel, V. Puech, A. Rousseau, in: *XIV ICGDA, Liverpool, GB (1–6 Sept. 2002)*. *Cont. papers*, vol. 2, pp. 40–43.
- [32] L. Magne, G. Baravian, S. Pasquiers, C. Postel, in: *11th Int. Symp. on Laser-Aided Plasma Diagnostics, Les Houches, France (28/09–2/10, 2003)*.
- [33] L. Magne, S. Pasquiers, C. Postel, in: *9th Int. Symp. on Non-Thermal Plasma (Hakone IX), Padou, Italy (23–26/08/2004)*.
- [34] L. Magne, J. Amorim, V. Edon, S. Pasquiers, F. Jorand, C. Postel, in: *57th Gaseous Electronics Conference, Bunratty, Ireland (26–29/09/2004)*.
- [35] F. Fresnet, G. Baravian, S. Pasquiers, C. Postel, V. Puech, A. Rousseau, M. Rozoy, *J. Phys. D* 33 (2000) 1315.
- [36] U. Rahmann, A. Büttler, U. Lenhard, R. Düsing, D. Markus, A. Brockhinke, K. Kohse-Höinghaus, *LASKIN—A simulation program for time-resolved LIF-spectra*, Internal Report, University of Bielefeld, Faculty of Chemistry, Physical Chemistry I, <http://pc1.uni-bielefeld.de/~laskin>.
- [37] W. Mallard, F. Westley, J. Herron, R. Hampson, D. Frizzell, *NIST chemical kinetics database (version 2Q98)*, 1998.
- [38] W. Tsang, R. Hampson, *J. Phys. Chem. Ref. Data* 15 (1986) 1087.
- [39] D. Baulch, D. Drysdale, D. Horne, A. Lloyd, *Evaluated Kinetic Data for High Temperature Reactions*, vol. 1: *Homogeneous Gas Phase Reactions of the H<sub>2</sub>–O<sub>2</sub> System*, Butterworths, London, 1972.